*Skin Research and Technology 2008; **14**: 152–164*
Printed in Singapore · All rights reserved
doi: 10.1111/j.1600-0846.2007.00269.x

Skin Research and Technology

A nonlinear elastic behavior to identify the mechanical parameters of human skin *in vivo*

A. Delalleau[1,2], G. Josse[2], J.-M. Lagarde[2], H. Zahouani[1] and J.-M. Bergheau[1]

[1]*Laboratoire de Tribologie et Dynamique des Systèmes, UMR 5513, CNRS, ECL, ENISE, Saint Etienne, France and* [2]*Skin Research Center, Pierre Fabre Research Institute, Toulouse, France*

Background/purpose: Various analyses have been performed to identify the mechanical properties of the human skin tissue *in vivo*. They generally use different approaches and hypotheses (behavior laws as well as mechanical tests) and the obtained results are consequently difficult to analyze and compare. In this paper, an inverse method that can be adapted to any kind of mechanical tests and behavior laws is presented.

Method: A suction deformation performed on the volar aspect of the forearm of a subject is considered. This test is modeled with the finite element method to compare the experimental and simulated curves using an inverse method that allows the skin mechanical parameters identification. This process is based on two optimization algorithms, Kalman's filter and Gauss–Newton's methods. To account for the nonlinear behavior of the skin, a specific nonlinear elastic law, which is then compared with standard linear elastic and neo-Hookean's mechanical behaviors, was developed.

Results: The obtained results first prove that neither linear elasticity nor neo-Hookean's laws can be used to model the skin. On the contrary, the nonlinear elastic model presents a relevant fit of the experimental curves. The skin thickness is also proved to be another key point to be taken into consideration.

Conclusions: The obtained results are successfully compared with literature and the reliability of the proposed method is underlined with the identification of 300 additional experimental curves. The different works we are currently focusing on are finally introduced.

Key words: Human skin – *in vivo* – suction test – finite element – inverse method – nonlinear elasticity

Accepted for publication 26 May 2007

HUMAN SKIN presents nonlinear viscoelastic anisotropic quasi-incompressible mechanical properties, which are difficult to study (1–4). The mechanical properties of living tissues are of potential interest in the identification of certain diseases, for assessing therapeutic intervention, or for predicting the effect of trauma. According to the literature, the dermis is assumed to be the principal structure contributing to the mechanical properties of the skin (1, 5–8). Several studies propose to analyze the single effect of each dermis ultra structure component. The study of the collagen, the elastin and the matrix of proteoglycans mechanics are of outstanding importance. However, to describe a reliable behavior for the skin, all these components need to be simultaneously taken into account (9).

The main component of the dermis is the collagen fibers (80% of the dermis dry weight), which present elastic properties (1, 4) (Young's modulus from 150 to 300 kPa according to Wilkes et al. (10) and up to 1 GPa according to Fung (3)). Their deformation mechanism is mainly responsible for the behavior of the skin. For small strains applied to the skin, the collagen fibers orientate in the direction of the stress (4, 10–13). The skin-related low stiffness is thus mainly due to the elastin mechanical properties Fig. 1(a) (4, 10, 11, 14, 15). For large strains, both collagen and elastin fibers are stressed, then the high elastic modulus of the collagen fibers modifies the elastic response of the skin, which becomes stiffer Fig. 1(a). Molinari et al. (13) and Silver et al. (14) propose to identify the collagen stiffness, thanks to the third phase slope Fig. 1(a). The collagen fibers are moreover assumed to be responsible for skin anisotropy (16–18), whereas the elastin fibers are involved in the prestress phenomenon (10, 14, 15). The viscosity of the skin is explained by the displacement of the interstitial

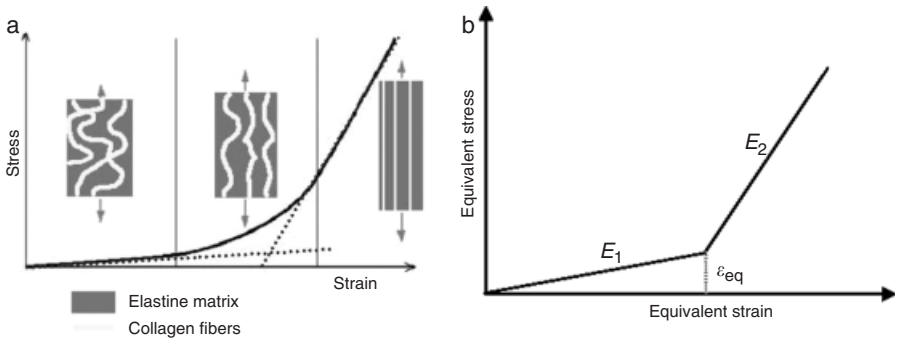

Fig. 1. (a) Nonlinear elasticity due to the orientation of the collagen fibers [HOLZ.200.2] (b) Corresponding numerical model. The nonlinear behavior law of the skin is characterized by only three parameters : E_1, E_2 and ε_{eq}.

fluid (10, 19), the shear interaction between collagen fibers and the matrix of proteoglycans (4), and the dissipative friction of the fibers (6, 8). Recent high-frequency ultrasound elastographic studies analyzed skin mechanical behavior, proving a complex interaction between these different components (20).

Many mechanical laws, which usually require complex backgrounds, have been analyzed to model soft tissues behavior *in vivo* (3, 4, 12, 19). Even if these formulations are based on physical assumptions their related parameters are generally difficult to analyze and identify (time-consuming algorithms, uniqueness of the solution, etc.). However, in clinical studies simple behavior laws are generally used and these have to be refined to perform a more reliable analysis of skin mechanics. Nevertheless, several authors proposed useful formulations in relation with the suction tests to evaluate the mechanical parameters of human skin. Diridollou et al. (21) assumed that the skin is a shell and identified its elasticity and prestress. Khatyr et al. (22) proposed to identify orthotropic properties of skin, thanks to Timoshenko's formulation (23). Kauer et al. (24) analyzed the mechanical properties of human uterus with compressible neo-Hookean and quasi-linear viscoelastic formulations. An extended incompressible neo-Hookean law is used by Hendricks et al. (25) to assess the mechanical properties of human skin. According to these studies, the nonlinearity of the skin behavior law seems to be a key point to better understand skin mechanisms. To account for the orientation of the fibers during stress, a two-slopes elastic numerical model is proposed with the advantage of being easy to use and simple to understand.

The skin needs to be tested *in vivo* to obtain reliable results for the identification of its mechanical parameters (1). First, the suction test principle is described. It is then modeled with the finite element method to draw a first comparison between two elastic behaviors: linear elasticity (Hooke's law) and hyperelasticity (neo-Hookean law). The presented results show that none of them are suitable to fit properly the suction curves. The nonlinear elastic formulation is thus introduced. As results mainly depend on the geometry of the tissue, numerical simulations were performed on a single-layer medium considering several thicknesses, which were measured using a high-frequency ultrasound device. The corresponding mechanical parameters are identified using a process based on two optimization algorithms: Kalman's filters (26–28) and Gauss–Newton's identification (29–31). These methods are briefly described, and the results related to the experimental curves are presented. Finally, some conclusions on the effects of skin thickness on the results are highlighted, and future developments we are currently working on are introduced.

Methods

This method is divided into three stages (26). First the experimental tests are performed and their measurements are gathered in a database named the *experimental space*. A *simulated space*, made up of numerical curves that are obtained for different values of the mechanical parameters, is then created. Finally, the actual mechanical parameters are identified by comparing the experimental and simulated spaces.

The suction test

The *in vivo* suction test (1, 5, 21, 22) consists of applying a negative pressure at the skin surface,

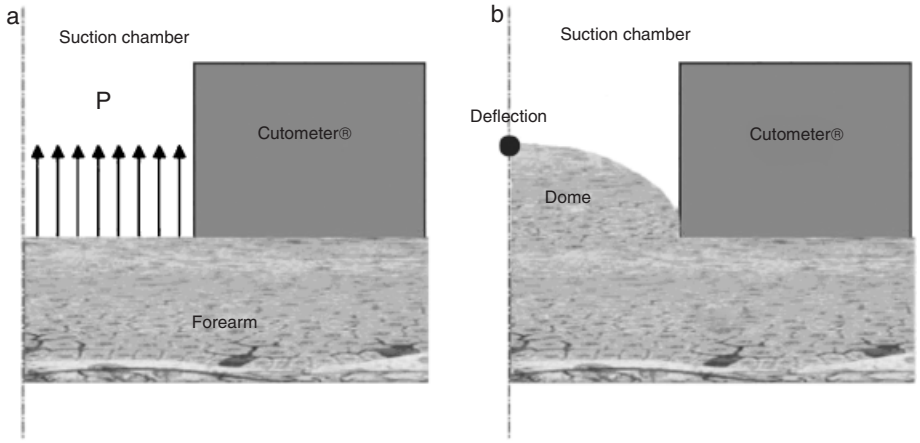

Fig. 2. Suction test. (a) Initial boundary and loading conditions. (b) Suction dome and deflection.

in this case on the volar aspect of the forearm skin, using a Cutometer CM570 (Courage & Khazaka, Cologne, Germany) Fig. 2(a). As a result, the skin is sucked into an aperture, forming a dome whose height is recorded Fig. 2(b). The studied experimental curves are presented in Fig. 3. The pressure applied is up to 100 mbar, at a rate of 20 mbar/s (the experimental curves obtained generally contain 50–100 points which are believed to be sufficient to perform mechanical computing). One-hundred and fifty tests were performed on 30 individuals, the thickness of the dermis for each experiment was measured using a high-frequency (20 MHz) ultrasound device (Dermcup, ATYS Medical, Soucieu en Jarrest, France) (32). The minimal value found was 860 μm Fig. 3(a) whereas the maximal one was equal to 1510 μm Fig. 3(c). To obtain a set of values for the individual forearm, both these thicknesses are considered for the study. The average value of the 150 measurements performed is about 1080 μm. A curve corresponding to this thickness was thus also considered. The experimental curves show a nonlinear trend, which can be interpreted as a change in the collagen orientation during the test (4, 10–13). For small strains, the skin presents low stiffness and the deflection rapidly increases with the pressure. For high strains – high pressure – the tissue becomes stiffer.

The simulated spaces – numerical models

The numerical simulations are performed with 2004 SYSTUS® finite element software (33). To model a complex medium such as skin, several assumptions were made:

(a) Skin is assumed to be a homogeneous medium.
(b) The mass inertial effects are neglected.
(c) The viscous and the anisotropic components are not considered. This approach thus consists of identifying the equivalent elastic properties of the skin.
(d) Owing to the axis of symmetry the geometry is considered to be axisymmetrical.

The dermis is assumed to be mainly responsible for the mechanical behavior of the skin (1, 5–8). Indeed, the hypodermis shows low-elastic properties (34, 35) and thus is on limited influence on the results. This hypothesis was also verified with ultrasounds imaging of the skin during a suction test (5), during suction deformation, subcutaneous structures do not affect the global response. The skin was thus simply modeled as a single-layer medium. Its thickness is the one related to the dermis. This assumption was also proposed by the literature (1, 22, 25).

The geometries of the three models (0.86, 1.08 and 1.51 mm) are presented in Fig. 4. The mesh is sufficiently wide so as to ensure that boundary conditions do not affect the distribution of strains in the zone where the pressure is applied. The displacement of the nodes related to the contact of the suction device and the skin are supposed to be null. The skin is meshed with second-order elements with a reduced integration scheme so as to avoid volumetric locking for quasi-incompressible problems ($045 \leq \upsilon < 0.5$). The present models include approximately 620 nodes and 190

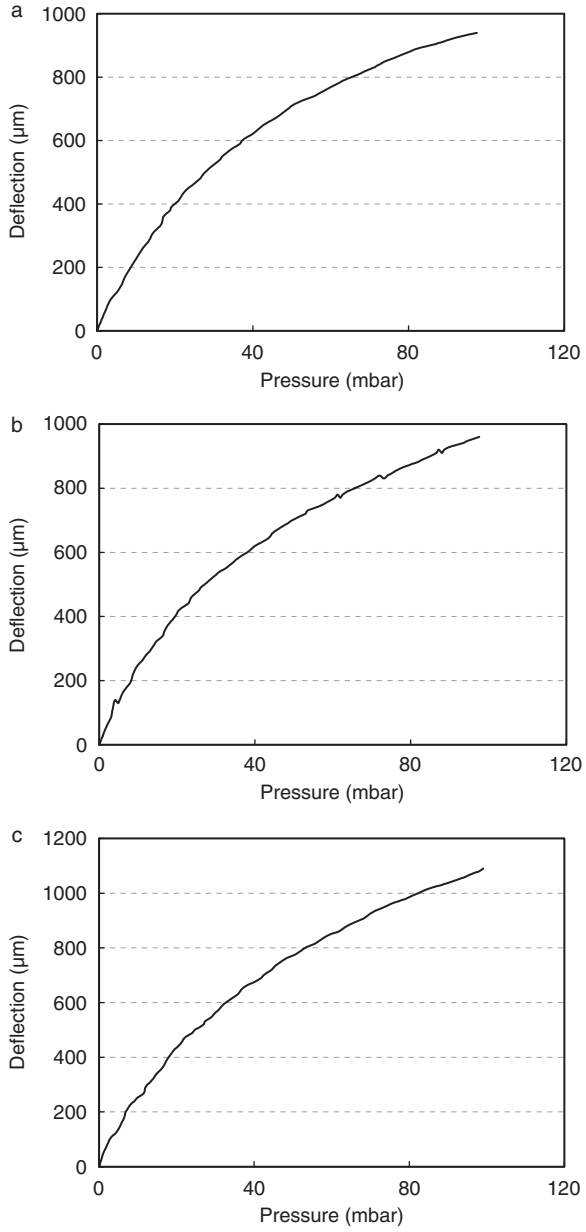

Fig. 3. The in vivo *experimental curves related the three measured thicknesses. (a) 0.86 mm. (b) 1.08 mm. (c) 1.51 mm.*

elements for thicknesses of 0.86 and 1.08 mm, and 740 nodes and 230 elements for the thickness of 1.51 mm. Three different elastic behaviors are studied.

Linear elasticity

Isotropic linear elasticity (36) can be defined for small displacements and small strains with Lamé's law $\boldsymbol{\sigma} = 2\,\mu\boldsymbol{\varepsilon} + \lambda \boldsymbol{tr}(\boldsymbol{\varepsilon})\mathbf{I}$, where $\boldsymbol{\sigma}$ is the stress tensor, $\boldsymbol{\varepsilon}$ is the linear strain tensor, $\mathbf{I}$ is the second-order identity matrix, $\lambda = E\upsilon/((1+\upsilon)(1-2\upsilon))$ and $\mu = E/(2(1+\upsilon))$ are Lamé's

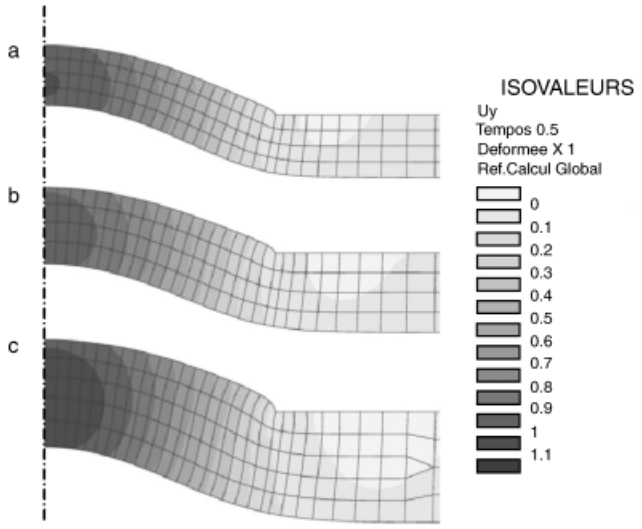

Fig. 4. Vertical displacements (µm) for three thicknesses. (a) 0.86 mm.(b) 1.08 mm (c) 1.51 mm.

coefficients, E the elasticity modulus (Young's modulus) and υ Poisson's ratio.

Neo-Hookean law

The conventional neo-Hookean law is defined by the potential $\boldsymbol{W} = X_1(I_1 - 3)$, where X_1 is a material constant and $I_1 = \boldsymbol{tr}(\mathbf{C})$ denotes the first invariant of the right Cauchy–Green deformation tensor $\mathbf{C}$. This law is defined for finite strains. Thus the second Piola–Kirchoff stress tensor is given by $\mathbf{S} = \partial W/\partial \mathbf{E}$, where $\mathbf{E}$ denotes the Green–Lagrange strain tensor.

Such a law is only available for incompressible media. A penalty method is generally used for the calculations. Nevertheless, Sussman and Bathe (37) propose a compressible potential for hyperelastic laws $\boldsymbol{W} = X_1(J_1 - 3) + (\kappa/2)(J_3 - 1)^2$, where κ is the compressibility constant, J_1 and J_3 are the first and third reduced invariant of the modified right Cauchy–Green deformation tensor $\mathbf{C}^* = I_3^{-1/3}\mathbf{C}$, where $J_3 = I_3^{1/2}$. As skin is generally assumed to be quasi-incompressible, (25, 38) the simple incompressible formulation is thus considered.

Nonlinear elasticity

Nonlinear elasticity (33) consists of a modification of the linear elastic Hooke's law for isotropic media. As the skin is assumed to be quasi-incompressible ($\upsilon = 0.45$), the effect of the bulk modulus is considered to be insignificant. Young's modulus then depends on the equivalent strain ε_{eq}, where $\varepsilon_{eq} = 1/(1+\upsilon)(3/2e_{ij}e_{ij})^{1/2}$ and e_{ij} are the

tensor components of the deviatoric part related to $\boldsymbol{\varepsilon}$. The elasticity is defined by different slopes. As suggested in the literature (4, 10–13), this model will be characterized by only two slopes [Fig. 1(b)], which are related to the first and third phases of the skin behavior law [Fig. 1(a)]. E_1 is the elasticity modulus that characterizes the first slope, E_2 is related to the second part.

The inverse method

The main advantage of the proposed method lies in the construction of a precalculation database: the *simulated space*. Indeed, clinical studies are performed with a large number of measurements. With the use of standard inverse methods, a finite element computation is required for each identification step. Redundant solutions to the numerical models are thus calculated. In the present procedure, all the finite element models are performed only one time. Furthermore, such experimentation is usually performed by medical practitioners, hence our method needs to be a FEM-free process. The results of several numerical calculations relating to the various mechanical parameters to be determined are collected in the simulated space. During the calculation, non-simulated values are computed with cubic Lagrange's interpolations of the existing data.

The proposed inverse method is based on two different algorithms: Kalman's optimization and Gauss–Newton's minimization. Kalman's filters, which were first described in 1960 (39), are based on a formulation similar to that of the recursive least squares: they involve minimizing an *a posteriori* identification error. The extended Kalman's filters (EKF), which propose a linearization of Kalman's equations, are used in this paper. For each step of pressure j, an estimate $\mathbf{x}_j^-$ of the mechanical parameters is calculated. $\mathbf{x}^{-T} = \{m_1^-, ..., m_n^-\}$, where m_k^-, with $k \in [1;n]$ are the n *a priori* mechanical parameters used to describe the behavior law. This estimate is then adjusted (Eq. 1), thanks to Kalman's gain matrix $\mathbf{K}_j$, which is weighted by the difference between the experimental deflection M_j and the simulated estimate S_j^-.

$$\mathbf{x}_j^+ = \mathbf{x}_j^- + \alpha \mathbf{K}_j (M_j - S_j^-) \tag{1}$$

The matrix $\mathbf{K}_j$ depends on the jacobian matrix corresponding to the simulated space. Further information can be found in Delalleau and colleagues (26–28, 39–41). In some cases the values of $\mathbf{x}_j^-$ can exceed the limits of the simulated space. This phenomenon generally leads to harmful numerical oscillations. The convergence is smoothed using a scalar parameter: $\alpha \in]0;1]$ (42), which can also be of great interest to reach the global minimum (e.g. line search).

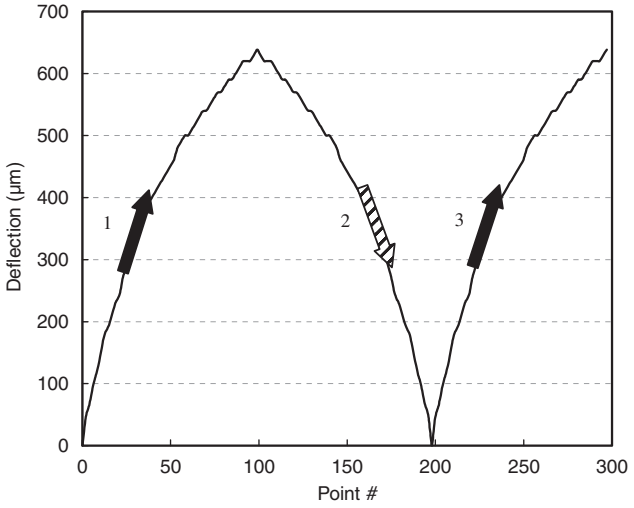

Fig. 5. Stabilization process. The curve is run using both the forward and reverse directions.

The required parameters cannot be identified with a single computation of the optimization process, hence a stabilization process is used. This method consists of an initial calculation with the proposed experimental curve (Fig. 5 step 1). The identification is then continued by considering the same curve in the reverse direction back to the point of departure (Fig. 5 step 2). Finally the experimental curve is run once again in the forward direction (Fig. 5 step 3). For all the iterations the parameters found are used to start the next calculation. A convergence criterion is then used to stop the process. This criterion is defined for a stabilization of the identified parameters between two consecutive forward iterations t of the stabilization process $\mathbf{C}_{t+1} = |\mathbf{x}_{t+1} - \mathbf{x}_t|$.

The standard Gauss–Newton algorithm (29–31) is based on the minimization of $\sum_{j=1}^{q} (M_j - S_j)^2$, where q is the number of experimental data points. For each iteration i it can be written as

$$\mathbf{x}_{i+1} = \mathbf{x}_i + \alpha \mathbf{G}_i \tag{2}$$

where $\mathbf{x}_i$ is the mechanical parameter identified for the ith iteration. $\mathbf{G}_i$ is defined as

$$\mathbf{G}_i = (\mathbf{F}_i \mathbf{F}_i^T)^{-1} \mathbf{F}_i^T (\mathbf{M}_i - \mathbf{S}_i) \tag{3}$$

where $\mathbf{F}_i$ is the jacobian matrix at iteration i, and $\mathbf{M}_i$ and $\mathbf{S}_i$ are the vectors that respectively contain

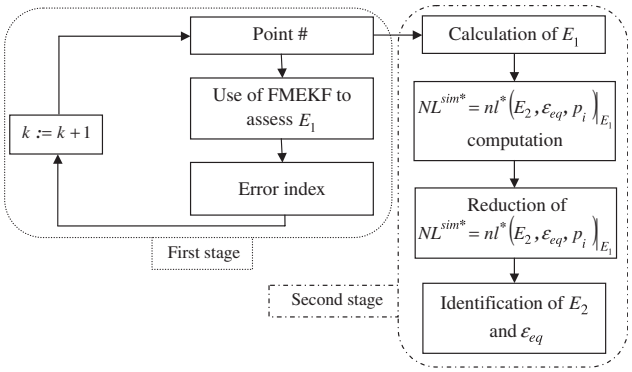

Fig. 6. Nonlinear algorithm. It is divided into two stages. The first one is related to the identification of E_1, thanks to Kalman's method. The second one allows the calculation of E_2 and ε_{eq}. In that case Gauss–Newton's algorithm is used.

the measured and simulated data points. The convergence C_{gn} is defined for a stabilization of the specified error $Er_i = \sum_{j=1}^{j} |M_j - S_j|$ between two consecutive iterations $C_{gn} = |Er_{i+1} - Er_i|$.

Kalman's algorithm constitutes a reliable and rapid explicit method. It is both less time and memory consuming than Gauss–Newton's minimization. The latter presents a better stability for the optimization simple problems. Both these methods were used to assess the mechanical parameters of the nonlinear behavior law that was developed.

The nonlinear identification algorithm

The nonlinear simulated space (simulated space corresponding to the nonlinear elastic behavior) is constructed for variations of the three parameters studied: $E_1 \in [20\,\text{kPa};290\,\text{kPa}]_{\text{step}=30\,\text{kPa}}$, $E_2 \in [100\,\text{kPa};1100\,\text{kPa}]_{\text{step}=100\,\text{kPa}}$ and $\varepsilon_{eq} \in [0.02;0.17]_{\text{step}=0.03}$. From now on, the nonlinear simulated space will be to referred as $NL^{\text{sim}} = nl\,(E_1, E_2, \varepsilon_{eq}, p_i)$, where p_i is the experimental steps of pressure. The identification is divided into two stages. Kalman's method was used for the first one and Gauss–Newton's algorithm for the second (Fig. 6).

The first stage consists in creating a *linear simulated space* (i.e. variations are only performed on E_1 with a standard linear Hooke's law). The experimental domains $M = [0;M_k]$ are successively reviewed, where $k \in [r;q]$, q is the number of points corresponding to the experimental curve, and r is the starting point, which is generally chosen equal to 5. Indeed, for lower values of r results are not reliable. For each of these $q-r$ domains, E_1^{id} is identified, thanks to Kalman's algorithm. This

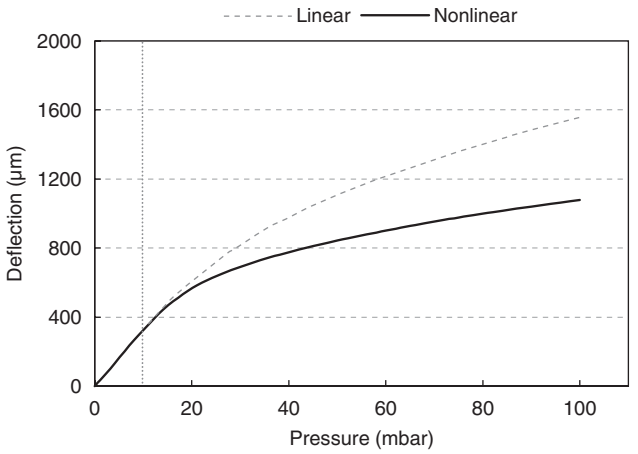

Fig. 7. Comparison between the linear and nonlinear formulations. They are in accordance for strains under the specified ε_{eq}. The mechanical properties are: $E_1^{\text{th}} = 110\,\text{kPa} = 110kPa$, $E_2^{\text{th}} = 500\,\text{kPa}$ and $\varepsilon_{eq}^{\text{th}} = 0.08$.

method was chosen here for its ability to rapidly review the experimental domains when Gauss–Newton's process is unable to do so. An error index related to M and $S(E_1^{\text{id}})$ is then calculated:

$$(\text{corr}_{k-(r-1)} = (1 - 1/k \sum_{j=r}^{k} (M_j - S_j)/M_j), k \in [r;q]),$$

where $\text{corr}_{k-(r-1)}$ is the error index calculated for the kth domain and ${}_{k-(r-1)}E_1^{\text{id}}$ is the corresponding identified parameter. As long as none of the elements of the mesh has reached the specified equivalent strain, standard linear elasticity and nonlinear elasticity are identical. A theoretical example is proposed in Fig. 7 with the thickness of 0.86 mm, and $E_1^{\text{th}} = 110\,\text{kPa}$, $E_2^{\text{th}} = 500\,kPa$, $\varepsilon_{\text{eq}}^{\text{th}} = 0.08$. For a pressure under 10 mbar the two results are equal. E_1 is identified for the maximum of the correlation index.

A new simulated space NL^{sim^*} is then constructed with Lagrange's cubic interpolations of the existing values of NL^{sim} for ${}_{k-(r-1)}E_1^{\text{id}}$:

$$\begin{aligned} NL^{\text{sim}} &= nl(E_1, E_2, \varepsilon_{\text{eq}}, p_i) \Rightarrow NL^{\text{sim}*} \\ &= nl^*(E_2, \varepsilon_{eq}, p_i)|_{{}_{k-(r-1)}E_1^{\text{id}}}. \end{aligned}$$

This domain is reduced using the pressure for which ${}_{k-(r-1)}E_1^{\text{id}}$ is defined. These two modifications make the calculation process faster. Gauss–Newton's minimization is then used to identify E_2^{id} and $\varepsilon_{\text{eq}}^{\text{id}}$ (Fig. 6).

As an example, the identification of the parameters previously defined (Fig. 7) is proposed. This is carried out using the following initial values: $E_1^{\text{init}} = 50\,\text{kPa}$, $E_2^{\text{init}} = 200\,\text{kPa}$ and $\varepsilon_{\text{eq}}^{\text{init}} = 0.02$. Figure 8 and Fig. 9 respectively show the variations of the error index and that

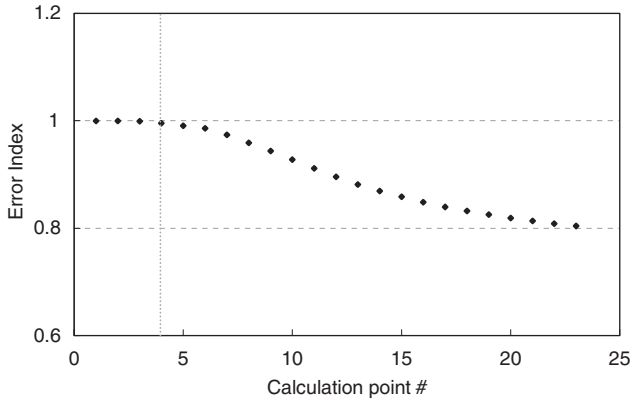

Fig. 8. Variations of the error index. The linear and nonlinear elastic behavior laws are in good accordance up to the third calculation point. These results are related to that of Fig. 6.

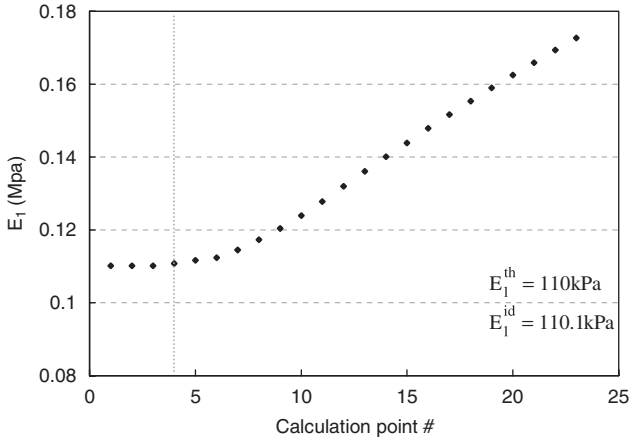

Fig. 9. Variations of corresponding Young's modulus E_1. These results are in agreement with the variations of the error index (Fig. 8).

of E_1 for the first calculation stage. As it is a theoretical case study, firsts solutions are identical (error index value at 1). First Young's modulus is consequently defined as the ones corresponding to maximum pressure. Figure 10 and Fig. 11 are related to the variations of E_2 and ε_{eq} for the second step of calculation. The required values are identified ($E_1^{id} = 110.1\,kPa$, $E_2^{id} = 499.1\,kPa$, $\varepsilon_{eq}^{id} = 0.08$) with an *identification error* $I_d = 0.21\,\mu m$, which is calculated as $I_d = (1/q)\sum_{j=1}^{q} |M_j - S_j|_{E_1^{id}, E_2^{id}, \upsilon^{id}}|$. The convergence criteria used for this computation are $C_k = 10^{-2}$ and $C_{gn} = 10^{-3}$ respectively, and the α parameter was chosen equal to 0.1. The efficiency of the identification is discussed in the results section.

Results

The current section first compares Hooke's and neo-Hooke's formulation while accounting for high strains and high displacements problems.

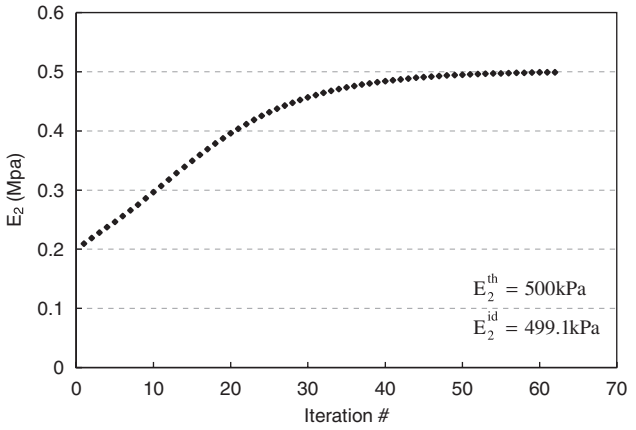

Fig. 10. Variations of Young's modulus E_2. Results show that this parameter reaches the required value $E_2^{th} = 500\,kPa$.

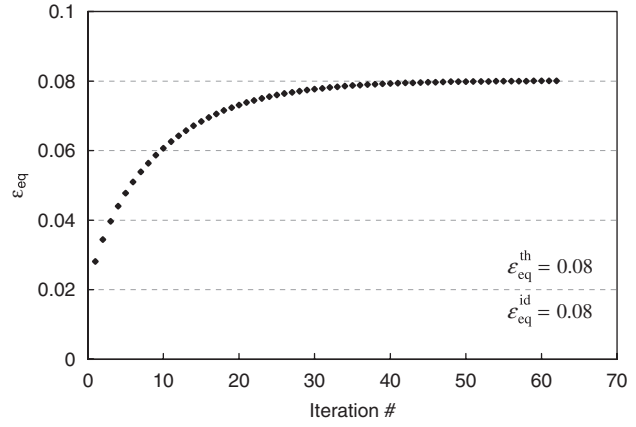

Fig. 11. Variations of the equivalent strain. Results show that this parameter reaches the required value ε_{eq}^{th}.

Elasticity vs. hyperelasticity

The study of the human skin mechanical properties is considered to be difficult to perform. Consequently, many authors use simple behavior laws such as the isotropic Hooke law. However, it is admitted that this formulation is only suitable for strains up to 5%. In the suction case study, the maximal component of the strains tensor can reach the value of 20%; hence, hyperelastic laws are more suitable. To account for high strains and displacements phenomena, geometrical nonlinearities have to be computed through two different formulations (36): the Total Lagrangian and the Updated Lagrangian ones.

The results of four finite element simulations are compared. The first one is related to Hooke's behavior law for small strains (*L*), the second one for Total Lagrangian formulation (*TL*), the third one uses an Updated Lagrangian formulation (*UL*) and the fourth study is related to a neo-Hookean behavior (*NH*) (Total Lagrangian

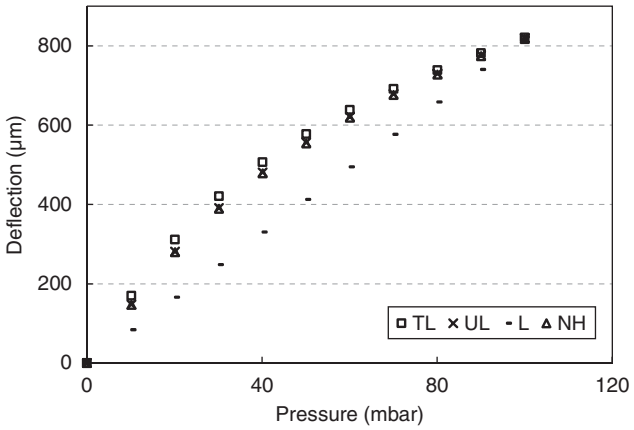

Fig. 12. Identification of the mechanical parameters for a non reliable thickness (0.5 mm). TL, Hooke's behavior law for Total Lagrangian formulation; UL: Hooke's behavior law for Updated Lagrangian formulation; L, standard Hooke's behavior law; NH, Neo-Hookean behavior law.

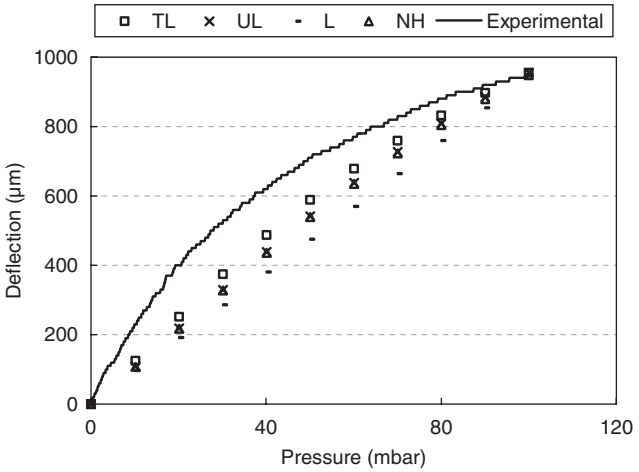

Fig. 13. Comparison of the simulated results for the 0.86 mm thickness. TL, Hooke's behavior law for Total Lagrangian formulation;. UL, Hooke's behavior law for Updated Lagrangian formulation; L, standard Hooke's behavior law; NH, Neo-Hookean behavior law.

formulation also). In the case of *TL* Hooke's law can be generalized to: $\mathbf{S} = 2\,\mu\mathbf{E} + \lambda \boldsymbol{tr}(\mathbf{E})\mathbf{I}$, where $\mathbf{S}$ is the second Piola–Kirchoff stress tensor and $\mathbf{E}$ is the Green–Lagrange strain tensor, whereas in the case of *UL* it can be written as $\boldsymbol{\sigma} = 2\,\mu\mathbf{D} + \lambda \boldsymbol{tr}(\mathbf{D})\mathbf{I}$, where $\boldsymbol{\sigma}$ is the Cauchy stress tensor and $\mathbf{D}$ is the Eulerian strain rate tensor.

A theoretical numerical model of 0.5 mm thickness is first studied. According to the literature (1) this skin thickness is not realistic for the forearm, but this test is useful for comparing the three Hookean formulations (*L*, *TL*, *UL*) and the neo-Hookean one (*NH*). Figure 12 proposes the comparison of the four simulated curves for the same maximum deflection. The results related to Hooke's law combined with the Total and *UL* are in good agreement with the neo-Hookean one. On the contrary the linear formulation (*L*) presents very different results. This indicates that the most important aspect of the suction test modeling is related to the large rotations and the large displacements phenomena. Consequently, for this thickness of 0.5 mm, geometrical nonlinearities can be used through Updated and *TL* to perform numerical calculations with a Hooke's behavior law. One can remark that geometrical nonlinearities also modify the shape of the simulated curves, which become nonlinear. Hence, their use is of potential interest to fit the experimental curves nonlinearities (Fig. 3). For larger, and therefore more realistic, skin thicknesses (usually from 0.8 to 2.5 mm (1)), strains and displacements usually present lower values. The previous conclusions can thus be extended to the study of standard suction tests. Identical analyses, whose results are presented in Fig. 13, Fig. 14 and Fig. 15 were drawn for the three considered thicknesses.

Table 1 illustrates the identified mechanical parameters for each formulation. For all the thicknesses, the corresponding results always present the same order of magnitude but none of the calculations is able to fit the experimental curves properly (Fig. 13, Fig. 14 and Fig. 15). This cannot be attributed to a lack in the identification process but to an inadequacy of the behavior laws, which propose a quasi-linear relationship between the pressure and the deflection for such strain levels. Whatever the formulation is, neither Hooke's nor neo-Hookean's laws is thus suitable to study the human skin mechanical properties.

Hendricks et al. (25) proposed to use an extended incompressible neo-Hookean law whose potential is expressed as $W = X_1(I_1 - 3) + X_2(I_1 - 3)(I_2 - 3)$. The results these authors obtained were in good agreement with their experimental curves. However, the considered model seems to be difficult to use to test skin aging or the effects of a treatment because a relationship between the mechanical parameters and the physiological phenomena is not straightforward. A simple two-parameters nonlinear elastic law is thus studied. It has been shown previously that in most of the suction case studies, Hooke's law can

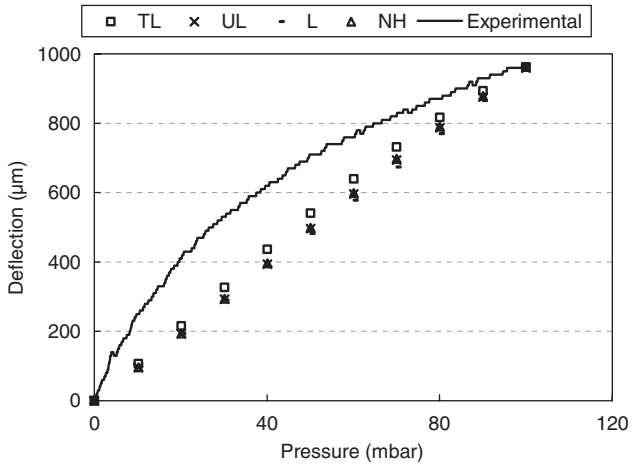

Fig. 14. Comparison of the simulated results for the 1.08 mm thickness. TL, Hooke's behavior law for Total Lagrangian formulation; UL, Hooke's behavior law for Updated Lagrangian formulation; L, standard Hooke's behavior law; NH, Neo-Hookean behavior law.

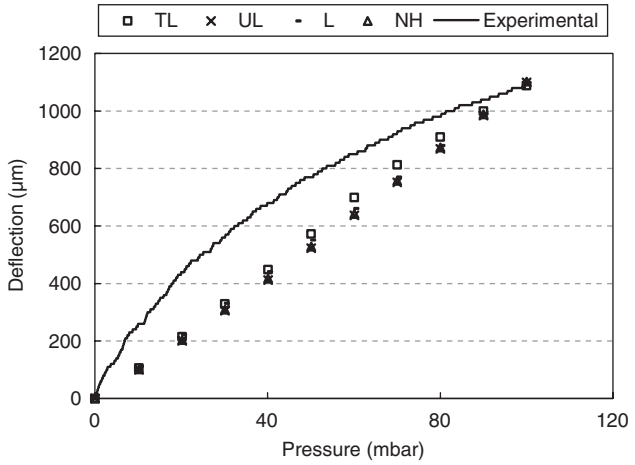

Fig. 15. Comparison of the results for the 1.51 mm thickness. TL, Hooke's behavior law for Total Lagrangian formulation; UL, Hooke's behavior law for Updated Lagrangian formulation; L, standard Hooke's behavior law; NH, Neo-Hookean behavior law.

TABLE 1. Values of the identified mechanical parameter (kPa)

	0.86 mm	1.08 mm	1.51 mm
TL	290	205	108
UL	360	226	114
L	330	215	100
NH	57	39	19

Ones can remark that for infinitesimal strains and quasi incompressibility $E = 6X_1$.

TL, Hooke's behavior law for Updated Lagrangian formulation; UL, Hooke's behavior law for Updated Lagrangian formulation; NH, neo-Hookean behavior law; L, standard Hooke's behavior law.

be extended with the use of geometrical nonlinearities. All the calculations are thus performed in a *TL* (better convergence abilities in comparison with the Updated Lagrangian one).

Nonlinear elasticity

First of all, the reliability of the algorithm to assess the equivalent elastic parameters of the experimental curve was tested. Table 2 shows the influence of the initial values on the results. This is presented for the 0.86 mm thickness but was also computed for the other two ones. For each initial value the identified parameters are almost identical. One can remark that Kalman's optimization shows a better reliability than Gauss–Newton's algorithm. Indeed, for each test the first identified parameters E_1^{id}(related to Kalman's algorithm) are equal to 131 MPa whereas the second ones, $E_2^{id}$and ε_{eq}^{id}(related to Gauss–Newton's method), show small variations. These results highlight the reliability of the presented identification method and may prove that, in most of the cases, a unique solution to the forward problem is identified.

The results related to the three thicknesses are presented in Table 3 and the comparisons between the experimental and the identified curves are shown in Fig. 16(a–c). The identified curves present a good fit of the experimental data. For this set of experimental curves, the Young modulus is lower for thicker skin (equal or higher deflection is observed for higher thickness). More studies taking into account individual information have to be performed. This behavior law can now be used to study the effects of aging on the skin mechanical properties.

Discussion

The main objective of this study was to define an identification method related to a new numerical model to account for the nonlinear behavior of human skin *in vivo*. A relationship between physiological and mechanical aspects is first drawn. The orientation of the dermis collagen fibers in the direction of the stress during an experiment involves changes in the elasticity of the skin, which becomes stiffer. This leads to a three-phase behavior law and justifies the nonlinear mechanical approach. Three experimental curves corresponding to minimal, average and maximal thicknesses of forearm dermis are considered. Experimental and simulated results are then compared through a specific inverse method based both on Kalman's and on Gauss–Newton's optimizations. The main advantage of the presented algorithm is that the mechanical parameters are identified regardless of the numerical simula-

TABLE 2. Reliability test for the actual case study ($C_k = 10^{-2}$, $C_{gn} = 10^{-3}$, $\alpha = 0.1$) for a thickness of 0.86 mm

E_1^{init}(kPa)	50	50	50	50	250	250	250	250
E_2^{init}(kPa)	200	1000	200	1000	200	1000	200	1000
ε_{eq}^{init}	0.03	0.03	0.15	0.15	0.03	0.03	0.15	0.15
E_1^{id}(kPa)	131	131	131	131	131	131	131	131
E_2^{id}(kPa)	365	370	365	367	365	370	365	367
ε_{eq}^{id}	0.038	0.037	0.038	0.037	0.038	0.037	0.038	0.037
l_d (μm)	10.8	11.2	10.8	10.7	10.8	11.2	10.8	10.7
NI	45	56	49	43	45	56	49	43

Ones can remark that the identified values related to Gauss–Newton's algorithm shows small variations.

TABLE 3. Identified values for the studied thicknesses

	Nonlinear elasticity			
Geometry (mm)	E_1(kPa)	E_2(kPa)	ε_{eq}(%)	l_d (μm)
0.86	131	365	3.8	10.8
1.08	64	273	3.9	15.1
1.51	41	187	6.8	10.6

The comparison between experimental and simulated curves is shown in Fig. 16.

tions. This is a fast and FEM-free process, which is a major advantage for its clinical use. Reliable mechanical parameters are finally identified.

This study was first intended to show that neither Hooke's nor neo-Hookean's laws suitable to study skin mechanical properties. It is then proved that, in most of the suction cases, the Total and Updated Lagrangian formulations can be applied to Hooke's law so as to account for high strains and high displacements. The studied strain level (maximum equivalent strain about 20%) allows a good correlation between the results related to the standard neo-Hookean's and Hooke's laws using geometrical nonlinearities. The TL has been chosen to run the calculations as it presents better convergence abilities for the nonlinear problem. The identified mechanical properties ($E_1 = 41$–131 kPa and $E_2 = 187$–365 kPa, see Table 3) are in agreement with the literature. For the suction test performed on individual's volar forearm, Agache et al. (43), Barel et al. (15) and Diridollou et al. (21) have respectively found Young's modulus about 250, 130 and 150 kPa. The values presented by Khatyr et al. (22) are about 140–1.85 Mpa (according to the orthotropic direction), and those related to Hendricks et al. (25) are 8.3 and 82.4 kPa (average values of an extended neo-Hookean law). The 0.86 and 1.08 mm experimental curves show a similar deflection. Then, if their thicknesses have not been measured, the identified parameters would have been equal. This underlines that thickness must be accounted for. This algorithm

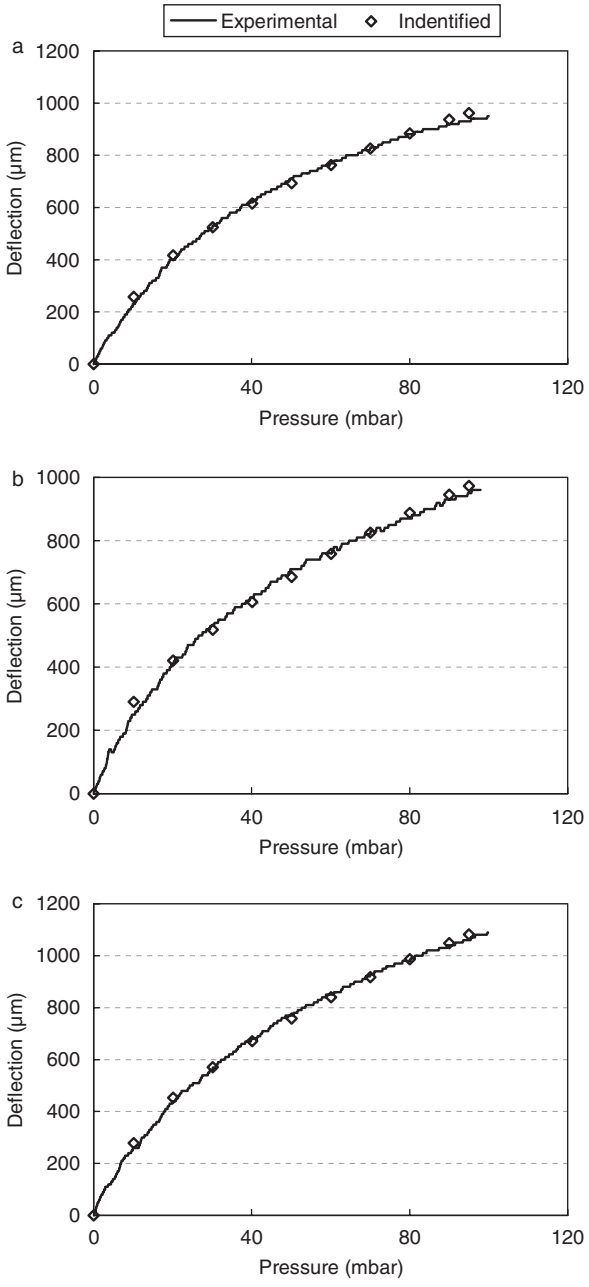

Fig. 16. Comparison between experimental curves and identified ones. (a) 0.86 mm ($E_1^{id} = 131$ kPa, $E_2^{id} = 365$ kPa, $\varepsilon_1^{id} = 131$ kPa). (b) 1.08 mm ($E_1^{id} = 64$ kPa, $E_2^{id} = 273$ kPa, $\varepsilon_1^{id} = 0.039$ kPa). (c) 1.51 mm ($E_1^{id} = 41$ kPa, $E_2^{id} = 187$ kPa, $\varepsilon_{eq}^{id} = 0.068$ kPa).

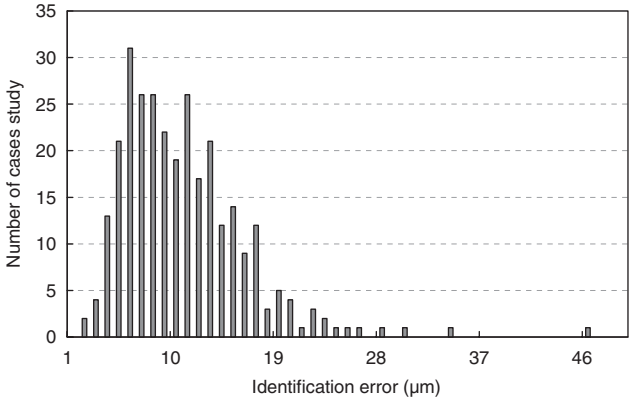

Fig. 17. Identification error related to 300 cases study. Only one calculation failed ($I_d = 46.1\,\mu m$).

should now be used to identify mechanical parameters related to several other experimental curves. Additional computations were successfully carried out on 300 experimental curves. Individual simulated spaces were constructed to account for the measured dermis thicknesses. This method will be developed in a future paper. Figure 17 presents the distribution of the identification error I_d. In most of the cases, identification errors are in agreement with Table 3 (six calculations present error values above 25 μm and one calculation failed). These conclusions highlight the reliability of both the nonlinear elastic behavior law and the proposed inverse method.

Even if nonlinearities are a major field of investigation, viscosity should also be considered (4, 6, 8, 10, 19). A new formulation of the algorithm we developed will thus be presented in future works. However, due to the high number of parameters, to determine the identification of skin viscoelastic properties is much more difficult.

Acknowledgements

The authors wish to thank Mr. J. Lipp (ENISE), Dr. R. Toscano (LTDS, UMR 5513, CNRS, ECL, ENISE) and Dr. D. Black (Institut de recherche Pierre Fabre) for their help.

Nomenclature

C_k = convergence criterion related to the Kalman's process
C_{gn} = convergence criterion related to the Gauss–Newton's process
$\mathbf{C}$ = right Cauchy–Green deformation tensor
$\mathbf{C}^*$ = modified right Cauchy-Green deformation tensor
$\mathbf{D}$ = Eulerian strain rate tensor
$\mathbf{E}$ = Green–Lagrange strain tensor
E = Young's modulus
E_i = Young's moduli related to the nonlinear behavior law
E_i^{id} = identified Young's moduli related to the nonlinear behavior law
E_i^{th} = theoretical Young's moduli related to the nonlinear behavior law
E_i^{init} = initial Young's moduli related to the nonlinear behavior law
Er_i = error related to Gauss-Newton's algorithm at iteration
$\mathbf{F}$ = Jacobian matrix related to Gauss–Newton's process
$\mathbf{G}$ = Gauss–Newton's matrix
I_i = invariants of the right Cauchy–Green deformation tensor
I_d = identification error
J_i = invariants of the reduced right Cauchy–Green deformation tensor
$\mathbf{K}$ = Kalman's gain matrix
M = experimental deflection
NL^{sim} = nonlinear simulated space
NL^{sim^*} = modified nonlinear simulated space
$\mathbf{S}$ = second Piola–Kirchoff stress tensor
S = simulated deflection
W = hyperelastic potential
$\mathbf{X}_i$ = material constants related to the hyperelastic models
corr = error index
$\mathbf{E}$ = deviatoric part of the linear strain tensor $\boldsymbol{\varepsilon}$
r = starting point related to the linear identification step
$\mathbf{x}^-$ = estimated mechanical parameters related to Kalman's calculation
$\mathbf{x}^+$ = adjusted mechanical parameters related to Kalman's calculation
α = scalar parameter used to reduce numerical oscillations of the optimization algorithms
$\boldsymbol{\varepsilon}$ = linear strain tensor
ε_{eq} = equivalent strain
ε_{eq}^{id} = identified equivalent strain
ε_{eq}^{th} = theoretical equivalent strain
ε_{eq}^{init} = initial equivalent strain
λ = first Lamé's coefficient
κ = compressibility material constant related to hyperelastic models

μ = second Lamé's coefficient
υ = Poisson's ratio
$\boldsymbol{\sigma}$ = Cauchy's stress tensor

References

1. Agache P. Physiology of the skin and cutaneous functional explorations. In: Tech Doc/Lavoisier, ed. Collection explorations fonctionnelles humaines, 2000: 407–441.
2. Reihsner R, Balogh B, Menzel EJ. Two-dimensionnal elastic properties of human skin in terms of an incremental model at the *in vivo* configuration. Med Eng Phys 1995; 17: 304–313.
3. Fung YC. Mechanical Properties of Living Tissues. Berlin: Springer, 1996.
4. Holzapfel GA. Biomechanics of soft tissues: handbook of material behaviour. Available at http://www.biomech.tugraz.at/papers/report7.pdf 2000: 12.
5. Diridollou S, Berson M, Vabre V et al. An *in vivo* method for measuring the mechanical properties of the skin using ultrasound. Ultrasound Med Biol 1998; 24: 215–224.
6. Silver FH, Freeman JW, DeVore D. Viscoelastic properties of human skin and processed dermis. Skin Res Technol 2001; 7: 18–23.
7. Dunn MG, Silver FH. Viscoelastic behaviour of human connective tissues: relative contribution of viscous and elastic components. Connect Tissue Res 1983; 12: 59–70.
8. Silver FH, Seehra P, Freeman JW, DeVores D. Viscoelastic properties of young and old human dermis: evidence that elastic energy storage occurs in the flexible regions of collagen and elastin. J Appl Polymers Sci 2002; 86: 1978–1985.
9. Pierard GE. EEMCO Guidance to the in vivo assessment of the tensile functional properties of the skin. Skin Pharmacol Appl Skin Physiol 1999; 12: 352–362.
10. Wilkes GL, Brown IA, Wildnauer RH. The biomechanical properties of skin. Crit Rev Bioeng 1973 453–495.
11. Daly CH. Biomechanical properties of the dermis. J Invest Dermatol 1982; 79: 17–20.
12. Bischoff JE, Arruda EM, Grosh K. Finite element modeling of human skin using an isotropic nonlinear elastic constitutive model. J Biomech 2000; 33: 645–652.
13. Molinari E, Fato M, De Leo G, Riccardo D, Beltrame F. Simulation of the biomechanical behavior of the skin in virtual surgical applications by finite element method. IEEE Trans Biomed Eng 2005; 52: 1514–1521.
14. Silver FH, Siperko LM, Seehra GP. Mechanobiology of force transduction in dermal tissue. Skin Res Technol 2003; 9: 3–23.
15. Barel AO, Courrage W, Clarys P. Suction method for measurement of skin mechanical properties: the cutomètre. In: Serup J, Jemec GBE, eds. Hand-book of non-invasive methods and the skin. Boca Raton: CRC Press, 1995: 335–340.
16. Langer K. Zue anatomie und physiologie de haut 1. ueber der spaltbarkeit der cutis. Sitzungsberich der Akademie der Wissenschaften in Wien. 1861; 44: PP. 19.
17. Manschot JFM, Wijn PFF, Brakee AJM. The angular distribution function of the elastic fibers in the skin as estimated from in vivo measurements. In: Nijhoff-Publisher M, ed. Biomechanics: principles and applications, 1982: 411–418.
18. Piérard GE, Lapière CM. Microanatomy of the dermis in relation to relaxed skin tension lines and Langer's lines. Am J Dermatopathol 1987; 9: 219–224.
19. Oomens CWJ, Van Campen DH, Grootenboer HJ. A mixture approach to the mechanics of skin. J Biomech 1987; 20: 877–885.
20. Mofid Y, Ossant F, Imberdis C, Josse G, Patat F. *In vivo* imaging of the skin under stesses: potential of high-freqency (20 MHz) static 2-D elastography. IEEE Trans Ultrason, Ferroelectrics Frequency Control 2006; 53: 925–935.
21. Diridollou S, Patat F, Gens F, Vaillant L, Black D, Lagarde J-M, Gall Y, Berson M. *In vivo* model of the mechanical properties of the human skin under suction. Skin Res Technol 2000; 6: 221–225.
22. Khatyr F, Imberdis C, Vescovo P, Varchon D, Lagarde J-M. Model of the viscoelastic behaviour of skin in vivo and study of anisotropy. Skin Res Technol 2004; 10: 96–103.
23. Timoshenko S, Woinowsky-Krieger S. Theory of plates and shells. New York: Mc Graw-Hill, 1964.
24. Kauer M, Vuskovic V, Dual J, Szekely G, Bajka M. Inverse finite element characterization of soft tissues. Med Image Anal 2002; 6: 275–287.
25. Hendricks FM, Brokken D, van Eemeren JTW, Oomens CWJ, Baijens JBAM, Horsten FPT. A numerical-experimental method to characterize the non-linear mechanical behaviour of human skin. Skin Res Technol 2003; 9: 274–283.
26. Delalleau A, Josse G, Lagarde J-M, Zahouani H, Bergheau J-M. Characterization of the mechanical properties of skin by inverse analysis combined with the indentation test. J Biomech 2006; 39: 1603–1610.
27. Welch G, Bishop G. An introduction to Kalman Filter. University of North Carolina at Chapel Hill. Available at: http://www.cs.unc.edu/~welch/media/pdf/kalman_intro.pdf.
28. Knight J. Computationally tractable SLAM. Report n°OUEL 2232/2001. Available at: http://citeseer.ist.psu.edu/565213.html. 2001.
29. Björck A. Least squares methods. In: Ciarlet PG, Lions JL, eds. Handbook of numerical analysis. North-Holland: Amsterdam, 1990: 465–647.
30. Fletcher R. Practical methods of optimization, 2nd edn. New York: John Wiley & Sons Inc, 1987.
31. Hartley HO. The modified Gauss–Newton method for fitting of nonlinear regression functions by least squares. Technometrics 1961; 3: 269–280.
32. Lagarde J-M, George J, Soulcié R, Black D. Automatic measurement of dermal thickness from B-scan ultrasound images using active contours. Skin Res Technol 2005; 11: 79–90.
33. SYSTUS® version 2004, User manual, ESI group.
34. Samani A, Bishop J, Yaffe M, Plewes DB. Biomechanical 3-D finite element modeling of the human breast for MR/X-ray using MRI data. IEEE Trans Med Imag 2001; 20: 4395–4405.
35. Schnabel JA, Tanner C, Castellano Smith AD, Leach MO, Hayes C, Degenhard A, Hose R, Hill DLG, Hawkes D. Validation of non-rigid registration using finite element methods. In: Insana MF, Leahy RM, eds. XVIIth international conference on information processing in medical imaging, lecture notes in computer science. New York: Springer Verlag, 2001: 2082.
36. Lemaitre J, Chaboche J-L. Mechanics of solid materials. Cambridge University Press, 1994: 123–162.

37. Sussman T, Bathe K-J. A finite element formulation for nonlinear incompressible elastic and inelastic analysis. Computer Struct 1987; 26: 357–409.
38. Schill MA. Biomechanical soft tissue modeling: techniques: implementation and applications. PhD Thesis, University of Mannheim. 2001.
39. Kalman RE. A new Approach to linear filtering and prediction problems. Trans ASME: J Basics Eng 1960; 82 (D): 35–45.
40. So CF, Ng SC, Leung SH. Gradient based variable forgetting factor RLS algorithm. Signal Proc 2003; 83: 1163–1175.
41. Zhang Y, Rong Li R. A fast U-D factorisation-based learning algorithm with applications to non linear system modelling and identification. IEEE Trans Neural Networks 1999; 10: 930–938.
42. Madsen K, Nielsen HB, Tingleff O. Methods for non linear least squares problems, informatics and mathematical modeling. Technical University of Denmark, 2nd Edition. Available at http://www2.imm.dtu.dk/courses/02611/nllsq.pdf. 2004.
43. Agache P. Noninvasive assessment of a biaxial Young's modulus of human skin *in vivo*. 9th International Symposium of Bioengineering and the Skin. 1992.

Address:
Gwendal Josse
Skin Research Centre
Pierre Fabre Research Institute
Hôtel Dieu Saint Jacques
2 rue Viguerie
31025 Toulouse
France

Tel: +33 5 6248 8515
Fax: +33 5 6248 8599
e-mail: gwendal.josse@pierre-fabre.com